Carlos M. C. G. Fernandes[1]
INEGI,
Universidade do Porto,
Campus FEUP,
Rua Roberto Frias 400,
Porto 4200-465, Portugal
e-mail: cfernandes@inegi.up.pt

Diogo M. P. Rocha
FEUP,
Universidade do Porto,
Rua Dr. Roberto Frias s/n,
Porto 4200-465, Portugal

Ramiro C. Martins
ISEP,
Instituto Politécnico do Porto,
Rua Dr. António Bernardino de Almeida, 431,
Porto 422-072, Portugal

Luís Magalhães
ISEP,
Instituto Politécnico do Porto,
Rua Dr. António Bernardino de Almeida, 431,
Porto 4200-072, Portugal

Jorge H. O. Seabra
FEUP,
Universidade do Porto,
Rua Dr. Roberto Frias s/n,
Porto 4200-465, Portugal

Hybrid Polymer Gear Concepts to Improve Thermal Behavior

A drawback of polymer materials is their low thermal conductivity which affects the operating temperature of polymer gears. The mechanical properties of a polymer gear are critically dependent on the maximum operating temperature. In order to improve thermal behavior of polymer gears, a hybrid polymer gear concept is suggested which consists of a polymer gear tooth with a metallic insert to promote heat evacuation from the meshing surface. The material selection based on finite element method (FEM) simulations showed that an aluminum insert performed better than copper and steel for a hybrid polymer gear. The results show that an aluminum insert increases the mass by 9% in comparison with a standard polymer gear but it decreases the maximum operating temperature by 28%. Insert geometries of different complexity were studied and their influence on operating temperature assessed. [DOI: 10.1115/1.4041461]

Keywords: hybrid polymer gears, bulk temperature, heat transfer, FEM

1 Introduction

The use of polymer gears is of great interest due to their potential advantages over metallic gears: the mass production is cheaper, they can operate without lubrication and are interesting for nonlubricated applications like printers, goods, and food industry applications. Polymer gears of the same size are lighter than steel gears thus can significantly reduce power consumption and noise level in gearboxes [1,2]. However, according to the literature, a thermal limit for polymer gears exists, usually a constant power for a certain application [3,4].

A major limitation, common to several polymer gear materials (like polyacetal and polyamide), is their low thermal conductivity [5], which can be improved using additives such as fibers, carbon nanotubes, or graphenes [6]. The use of such additives needs to be properly balanced to assure that improved thermal properties do not affect negatively the tribological performance (coefficient of friction and wear), decreasing in this way the main advantage of such materials—their self-lubrication capability [7]. Yet, other advanced materials might be used: variations of polyacetal (POM), polyamide (PA), or polyether-ether-ketone (PEEK) that present higher thermal capacity, although at a significantly higher cost.

The poor thermal conductivity of polymer gears results in poor heat conduction and high tooth contact temperature. This situation may be overtaken using: (i) metallic inserts impregnated in the polymer matrix that will promote a better heat conduction, decreasing the operating temperature and increasing the load carrying capacity, and (ii) improving gear tooth geometry to decrease the power loss and the heat generated between the contacting teeth [8–14].

Manufacturing of hybrid polymer gears is still not common. Different manufacturing processes (common in other applications) will be required to produce hybrid polymer gears. "Overmolding," a polymer injection molding process where one material is molded onto a second material, being two common technologies: (a) "insert molding," where an insert previously injected or machined is over molded by a plastic material, and (b) "multimaterial molding," where different polymer materials can be injected in the same production cycle [15]. Another manufacturing procedure, designated as "after molding" technology and consisting in the fixation of a metallic component over a polymer matrix by ultrasound welding or other similar process, may also be used.

The scientific and technological problems associated with the production of hybrid polymer/metal components, with very different physical and mechanical properties (polymers and metals) are significant, requiring significant research and development. However, the application field of polymer gears will grow significantly with hybrid polymer gears.

Finite element method (FEM) solutions for the thermal behavior of gears were proposed in several studies [16–19]. In a previous work [20], the authors validated a FEM model able to predict bulk and flash temperature both on lubricated and dry conditions and for different gear materials (steel, polymer).

The present work intends to study the influence of a metallic insert on the thermal behavior of a nonlubricated polymer gear, i.e., a hybrid polymer gear. The main goal is then to decrease the maximum temperature because the mechanical properties (mechanical strength) of the polymer are greatly influenced by the

[1]Corresponding author.

Contributed by the Tribology Division of ASME for publication in the JOURNAL OF TRIBOLOGY. Manuscript received January 17, 2018; final manuscript received September 7, 2018; published online November 13, 2018. Assoc. Editor: Sinan Muftu.

operating temperature. The insert geometry and its material are also studied in the present work and some possible hybrid polymer gear geometries are suggested.

2 Hybrid Polymer Gear Concept

A hybrid polymer gear consists of a polymer gear with a metallic insert (or any other candidate material with good thermal conductivity and adequate mechanical properties). A general approach for this study starts with a simple insert in the shape of a rectangular block in the middle of the teeth, as shown in Fig. 1, so the symmetry condition over the Cartesian axis of the three-dimensional gear tooth model is assured.

The implementation of an insert inside a polymeric gear presents several technological challenges like the thermal contact between bodies, the mechanical adhesion between them, and the manufacturing challenges that emerge.

Moreover, it is known that plastic gears' mechanical resistance properties are highly dependent on the operating temperature of the gear, being mandatory to control its maximum temperature. Therefore, it is important to study how the bulk temperature is influenced by the metallic insert inside the gear tooth.

In terms of FEM analysis, the insert implies a new boundary condition between metal and plastic. The study of heat transfer mechanisms between two bodies is then the main problem in FEM analysis.

The contact between the polymer body and the metallic insert which is a thermal contact resistance (TCR) is influenced by many factors like the roughness and waviness of the contacting surfaces (in case of flat, wavy-smooth, or even wavy-rough surface) or the effect of the existence of oxides at the contacting surface level [21].

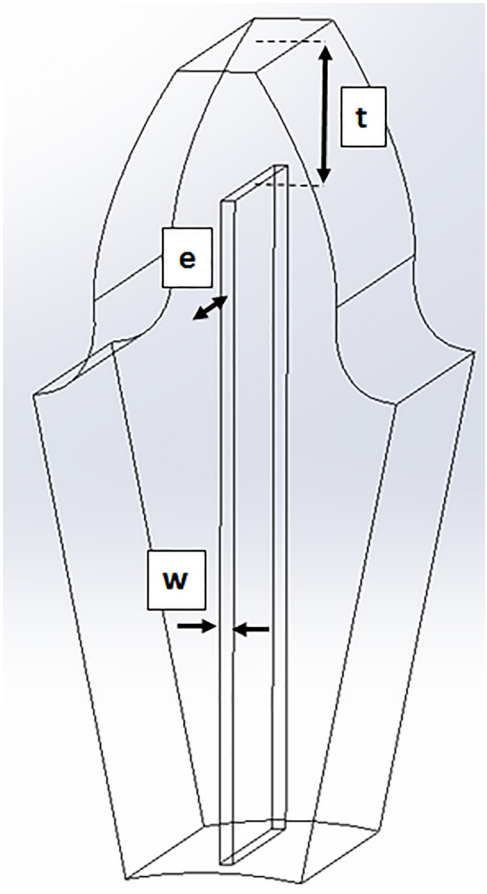

Fig. 1 Geometrical parameters of the basic hybrid-gear model

The microscopic analysis of machined surfaces allows to observe some defects at a microscale that result from the tool shape, the machining process, or even from the mold itself (also known as roughness) or even at a larger scale due to the heat treatment or vibration during manufacturing process. The imperfections of the surface geometry create a connection at specific points of the interface between the two bodies in contact instead of the contact between two theoretical surfaces.

3 Heat Transfer Coefficient in the Polymer/Metal Interface

3.1 Thermal Contact Between Two Bodies. The thermal contact conductance/resistance between the temperature drop (as shown in Fig. 2(*a*)) and the heat flux that passes at the apparent cross section area is required to determine the temperature distribution between two thick solid bodies. The thermal resistance is given by the Eq. (1):

$$R_{tc} = \frac{\Delta T_c}{Q \cdot A_a} \tag{1}$$

Then, the total heat transfer contact coefficient, h_{tc}, is a function of three physical phenomena (see Fig. 2(*b*)): conduction through the contacting points (h_c), radiation through the gaps between the

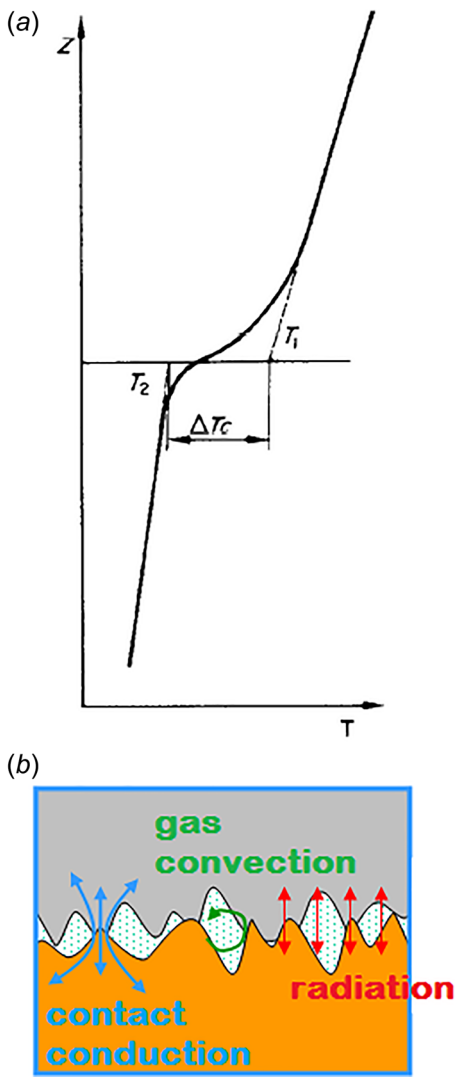

Fig. 2 Temperature drop and fundamentals modes of heat transfer at thermal joint between two bodies: (*a*) temperature drop [22] and (*b*) modes of heat transfer [23]

two surfaces (h_{rad}), and gas convection through the gas that fills these gaps (h_g), as shown in the Eq. (2):

$$h_{tc} = h_c + h_{rad} + h_g \tag{2}$$

Assuming that a hybrid polymer gear can be manufactured by molding, the heat transfer through the gas that fills the gaps between the two surfaces will be negligible since the gaps are very small. For the same reason, the heat transfer due to the radiation may also be neglected. So, the only heat transfer mode that will be taken into consideration is conduction through the contacting points: $h_{tc} = h_c$.

The heat transfer through the contact is complex depending on several parameters established by mechanical, thermal, or geometric properties of the contacting surfaces. The thermal contact resistance is influenced by the gap thickness, the waviness, the roughness of the contacting bodies, and the thermal conductivity of the solids. Therefore, the following simplifications are used: the contact is static, no vibrational effect is present, and the solids in contact have isotropic thermal and physical properties [21].

3.1.1 Effective Surface. To model the thermal contact conductance, some parameters are required in advance: the root mean square roughness σ or R_q, and the absolute asperity slope m_a, given by the following equations:

$$\sigma = \sqrt{\frac{1}{L}\int_0^L y^2 dx} \tag{3}$$

$$m_a = \frac{1}{L}\int_0^L \left|\frac{dy}{dx}\right| dx \tag{4}$$

If the heights of the two contact surfaces follow a Gaussian distribution, the problem can be approximated by a single rough surface contacting with a smooth surface (theoretical surface) as shown in Fig. 3.

The two parameters, discussed previously (effective root-mean-square roughness, σ_s, and effective absolute mean asperity slope, m_s) [25], are calculated with the following equations:

$$\sigma_s = \sqrt{\sigma_1^2 + \sigma_2^2} \tag{5}$$

$$m_s = \sqrt{m_1^2 + m_2^2} \tag{6}$$

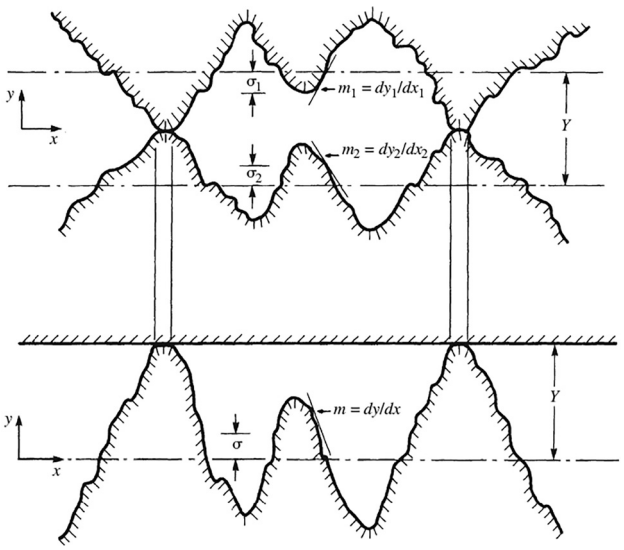

Fig. 3 Transformation of two contact surface into one rough surface with Ref. [24]

3.1.2 Initial Studies of Heat Flow Channel and Thermal Contact Resistance. The initial study of the heat flow between two solid bodies was based on the model shown in Fig. 4, which was simplified by Centinkale and Fishenden into a cylinder model [26]. These results show that although the two cylinders may have different conductivity, the heat is also conducted from the interstitial gap (adiabatic plane, $z = 0$, see Fig. 2(*a*)).

In practice, there is not only one single contact area between the two solid bodies. In fact, the contact may be composed of multiple contact areas, distributed over an apparent area of contact (A_a). Yovanovich [27] proposed a general thermal model for conforming rough surfaces, which describes the constrictions and resistance of a single asperity in contact and extends it to the whole surface. For a single contact spot (i) of the contact between two general surfaces (1 and 2), Eq. (7) can be used to determine the contact resistance

$$R_{si} = \frac{\psi_{ci_1}}{4 \cdot k_1 \cdot a_i} + \frac{\psi_{ci_2}}{4 \cdot k_2 \cdot a_i} \tag{7}$$

Taking into consideration the effective conductivity, due to the symmetry at the interface, $k_s = 2 \cdot k_1 \cdot k_2/(k_1 + k_2)$, Eq. (7) can be transformed into the Eq. (8):

$$R_{si} = \frac{\psi_{ci}}{2 \cdot k_s \cdot a_i} \tag{8}$$

Finally, to calculate the thermal contact conductance, Eq. (9) is used

$$h_c = 2 \cdot k_s \cdot \frac{1}{\psi_{ci}} \cdot \frac{a_i}{b_i} \tag{9}$$

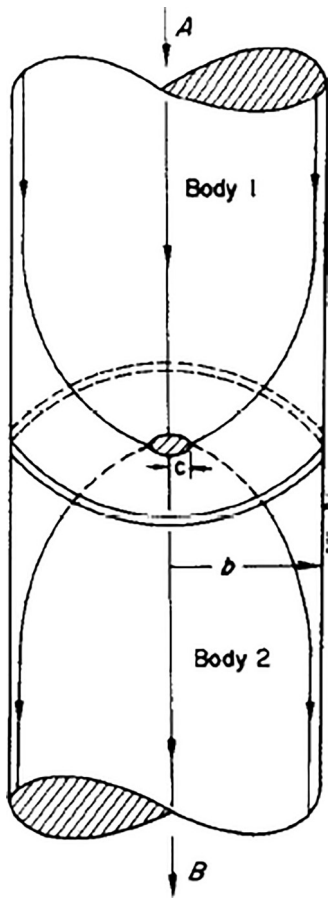

Fig. 4 Elemental flow channel [22]

The contact spot constriction parameters are given by the Eq. (10):

$$\psi_{ci_1} = \psi_{ci_2} = \psi_{ci} = (1-\varepsilon)^{1.5} \tag{10}$$

where $\varepsilon = \frac{a_i}{b_i} = \sqrt{A_r/A_a}$ is the ratio between the real area of contact (A_r) and the apparent area of the contact.

3.2 Thermal Models. The constant need to describe and to understand the problem of thermal contact conductance leads to the formulation of a large number of models and equations. The following modeling situations might be considered regarding the contacting bodies: elastic (small bodies), plastic (large contact strain), or elasto-plastic (combination of both).

For the present work, it was assumed that an elastic model is the most realistic situation to consider for the hybrid polymer gear concept.

The most common models to determine the heat transfer in the contact area for plastic or elasto-plastic situations are described in Appendices A and B, respectively.

3.2.1 Elastic Contact Model. Mikic [28] was able to determine that the elastic deformation is proportional to the pressure in the polymer metal interface according to the Eq. (11):

$$\frac{A_r}{A_a} = \frac{P}{H_e} \tag{11}$$

Similar to the plastic microhardness introduced by Yovanovich [27], the elastic microhardness (H_e) is calculated with the Eq. (12):

$$H_e = \frac{E^* \cdot m_s}{\sqrt{2}} \tag{12}$$

The effective elastic modulus (E^*) is calculated with the Eq. (13):

$$E^* = \frac{E_1 \cdot E_2}{E_2 \cdot \left(1-\nu_1^2\right) + E_1 \cdot \left(1-\nu_2^2\right)} \tag{13}$$

The equation of the dimensionless thermal contact conductance for a relative pressure range interval between $10^{-5} \leq P/H_e \leq 0.2$ is given by the Eq. (14):

$$C_c = \frac{h_c \cdot \sigma_s}{k_s \cdot m_s} = 1.54 \cdot \left(\frac{P}{H_e}\right)^{0.94} \tag{14}$$

Later on, Fuller and Marotta [29] suggested the change of the elastic contact hardness H_e for the polymer elastic contact hardness, H_{poly}, as presented in the Eq. (15):

$$H_{\text{poly}} = \frac{E_{\text{poly}} \cdot m_s}{2.3} \tag{15}$$

For polymers, Eq. (16) can be used to calculate the dimensionless thermal contact conductance

$$C_c = \frac{h_c \cdot \sigma_s}{k_s \cdot m_s} = 1.49 \cdot \left(\frac{P}{H_{\text{poly}}}\right)^{0.935} \tag{16}$$

Finally, the heat transfer coefficient may be obtained using the Eq. (17):

$$h_c = 1.49 \cdot \frac{k_s \cdot m_s}{\sigma_s} \cdot \left(\frac{P}{H_{\text{poly}}}\right)^{0.935} \tag{17}$$

The heat transfer coefficient due to the thermal contact resistance between the polymer and the metallic insert was predicted considering different contact pressures. The TCR (and the heat transfer coefficient) is dependent on the contact pressure between the polymer and the metallic insert. According to experimental investigations, the thermal resistance will vary with the contact pressure as shown in Table 1 for metal/metal interfaces [30]. A similar effect of pressure on the thermal resistance would be observed for polymer/metal interfaces due to the fact that in both cases the contacting surfaces are rough.

Table 1 Thermal resistance ($R_{tc} \times 10^{-4}$ (m^2 K W^{-1})) for a metal/metal interface under vacuum conditions [30]

Contact pressure	0.1 MPa	10 MPa
Stainless steel	6–25	0.7–40
Copper	1–10	0.1–0.5
Magnesium	1.5–35	0.2–0.4
Aluminum	1.5–5.0	0.2–0.4

Table 2 Geometry of the spur polymer gear used for the simulations [11]

Property	Pinion		Wheel
Number of teeth, z	16		24
Module, m (mm)		4.5	
Center distance, a (mm)		91.5	
Pressure angle, α (deg)		20	
Face width, b (mm)		14	
Addendum modification, x_z	+0.1817		+0.1715
Addendum diameter, d_a (mm)	82.64		118.54
Transverse contact ratio, ϵ_α		1.44	
Average roughness, Ra (μm)		0.5	
Material		POM	

4 Finite Element Method Implementation

In a previous work, a FEM model to predict both bulk and flash temperature in standard polymer gears was implemented and validated [20]. In the present analysis, only the bulk temperature was considered critical for the analysis and a steady-state model was used.

The bulk temperature, in a point far away from the thermal skin, is assumed to remain constant at any point of the gear as the time required for one revolution of a gear is smaller than the time needed for any change in the gear bulk temperature. Equation (18) governs the bulk temperature distribution within the solid, $T_B = T_B(x, y, z)$

$$k \cdot \left(\frac{\partial^2 T_B}{\partial x^2} + \frac{\partial^2 T_B}{\partial y^2} + \frac{\partial^2 T_B}{\partial z^2}\right) = 0 \tag{18}$$

For a complete description of the FEM model, refer to Ref. [20].

Since the polymer's mechanical properties are highly dependent on temperature, a hybrid gear with a metallic insert was designed to improve the bulk temperature distribution (Fig. 1).

The polymer gear in contact with the insert shares a boundary condition for the inner hole of the shaft, an adiabatic boundary condition as described in a previous work [20]. The implementation of the model is done in open-source FEM code ElmerFem®.[2] The contact between the polymer and the insert is a thermal contact resistance, implemented as a heat gap boundary condition with the corresponding heat transfer coefficient between the contacting surfaces (thermal contact) defined by Eq. (17). An elastic contact model was considered for the present analysis as described before.

An important aspect to keep in mind to solve the FEM problem is that, in the contact zone between the polymer body and the

[2] http://www.csc.fi/elmer

Table 3 Mechanical and thermal properties of different materials (POM at 40 °C) [35,36]

Properties	Copper	Aluminum	Steel	POM
Young's modulus, E (GPa)	107	69	206	2.69
Poisson's ratio, υ	0.36	0.33	0.30	0.30
Density, ρ (kg m^{-3})	8933	2702	7870	1410
Thermal conductivity, k (W m^{-1} K^{-1})	401.0	237.0	41.8	0.3
Specific heat, c (J kg^{-1} K^{-1})	385	903	493	1470
Dry coefficient of friction, μ (POM/POM) [36]	—	—	—	0.21

Table 4 Operating conditions

Operating conditions	
Torque of the pinion shaft (N·m)	10
Pinion rotational speed, n (rpm)	1000
Ambient temperature, T_{amb} (°C)	15

Table 5 Maximum and minimum temperature for a contact pressure of 25 MPa

POM without insert	T_{max} (°C)	139.4
	T_{min} (°C)	22.3
Aluminum insert	T_{max} (°C)	128.3
	T_{min} (°C)	35.0
Copper insert	T_{max} (°C)	128.2
	T_{min} (°C)	35.0
Steel insert	T_{max} (°C)	131.0
	T_{min} (°C)	34.8

metallic insert, the temperature should be equal (see Fig. 2(*a*)). However, creating this two volume problem (hybrid gear), the problem only has a numeric solution if the nodes in the polymer surface are made coincident with the nodes on the metallic surface.

The FEM mesh for the polymer gear and the insert bodies was created on Gmsh, but they are unstructured meshes [31]. So, in order to equalize the temperature solution values of each pair of contacting boundary condition, the FEM code needs a duplicated node for interface contact node, i.e., a node with the same coordinates duplicated on each body.

The standard polymer gear geometry considered for the FEM analysis is a spur gear with the geometric characteristics presented in Table 2. This geometry was selected because it allows the use of a common FZG gear test rig (Strama-Michaelis, Straubing, Germany) in order to perform experiments [32–34]. The polymeric gear material used is a common POM, with the physical properties described in Table 3. The mechanical and thermal properties of the candidate insert materials aluminum, copper, and steel are also presented in Table 3.

For what follows, the operating conditions described in Table 4 were used.

Table 6 Mass for one pinion tooth (calculated)

Material	Insert mass (g)	Total mass (g)
POM without insert	—	4.208
Aluminum insert	0.251	4.329 (+2.88%)
Copper insert	0.826	4.904 (+16.54%)
Steel insert	0.714	4.792 (+13.88%)

5 Simple Plate Insert

5.1 Influence of the Insert Material. To study the influence of the material and the contact pressure of the insert on the maximum bulk temperature of the hybrid polymer gear, a simple metallic insert was studied with the following geometric characteristics: $w_x = 0.1 \cdot m = 0.45$ mm, $e = m/2 = 2.25$ mm (for each side), and $t = m = 4.5$ mm, refer to Fig. 1. The FEM mesh has 688,384 elements for the tooth body and 104,219 elements for the insert body.

For the same contact pressure, 25 MPa, Table 5 shows that for different insert materials, a small difference in the maximum temperature result is observed. The maximum temperature is inversely proportional to the thermal conductivity while the minimum temperature, achieved in a position far away from the meshing surface, is lower for lower thermal conductivity. The thermal conductivity itself explains why a POM gear without insert presents higher maximum temperature, but much lower minimum temperature at the same time, i.e., the gradient is much higher for a standard polymer gear. The minimum temperature is not a problem in the present study, since the main goal is to decrease the maximum temperature because the mechanical properties of the polymer material will improve, therefore possibly increasing the load carrying capacity of polymer gears.

5.1.1 Influence of the Insert Material on the Tooth Mass. A brief analysis of the influence of the insert material on the mass of a single tooth was performed and compared with the standard POM solution, as presented in Table 6, where the middle column

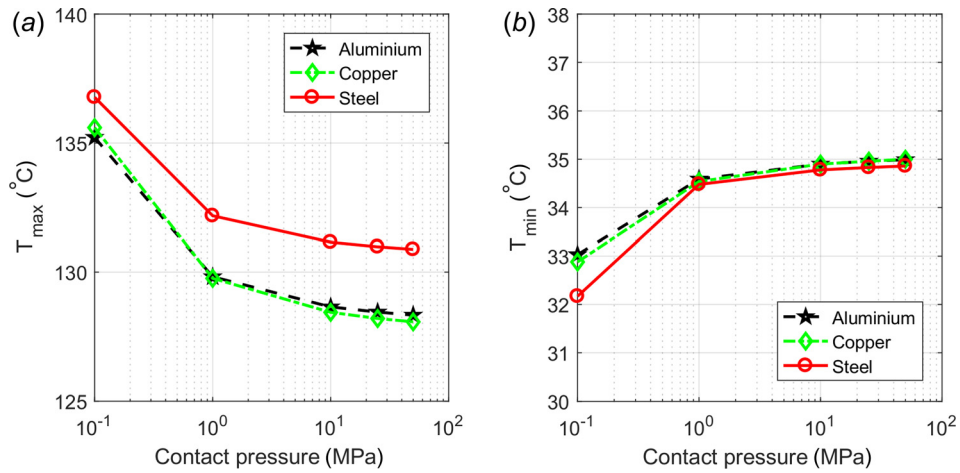

Fig. 5 Maximum and minimum temperature for each material for the first hybrid gear model: (*a*) maximum temperature for each material and (*b*) minimum temperature for each material

shows the mass of the insert and the final column shows the total mass of the pinion tooth. The metallic insert promotes a decrease of the maximum temperature, but implies an increment of approximately 3% in the tooth weight if aluminum is used, and 17% or 14% if copper or steel is chosen, respectively.

5.1.2 Influence of the Contact Pressure Between Polymer and Metallic Insert. Figures 5(*a*) and 5(*b*) show the maximum and the minimum temperature for each thermal contact resistance (which is imposed by the contact pressure). In summary, the steel insert has the highest maximum temperature no matter the contact pressure selected, as shown in Sec. 5.1.1.

Since the contact pressure depends on the manufacturing process, its value is unknown. However, the simulation results show that after 10 MPa, the increase in heat transfer coefficient due to the decrease in the thermal contact resistance will not change significantly the maximum and minimum temperatures of the gear tooth. This suggests that the heat evacuation limitation is in the geometry of the insert more than on the contact pressure. Thus, if a minimum contact pressure between the gear body and the metallic insert is assured (>10 MPa), the heat evacuation by the insert is efficient enough.

Figure 6 show the influence of the contact pressure (0.1 MPa, 10 MPa, and 50 MPa) on the gradient of bulk temperature of both gear and insert. The increase of the contact pressure changes the gradient within the metallic insert. However, comparing the result from 10 MPa to 50 MPa, the difference is negligible.

The insert is able to evacuate a higher heat flux with increased interface pressure and, therefore, reduce the maximum temperature. However, the heat is conducted to the colder part of the tooth, and consequently, the minimum temperature rises.

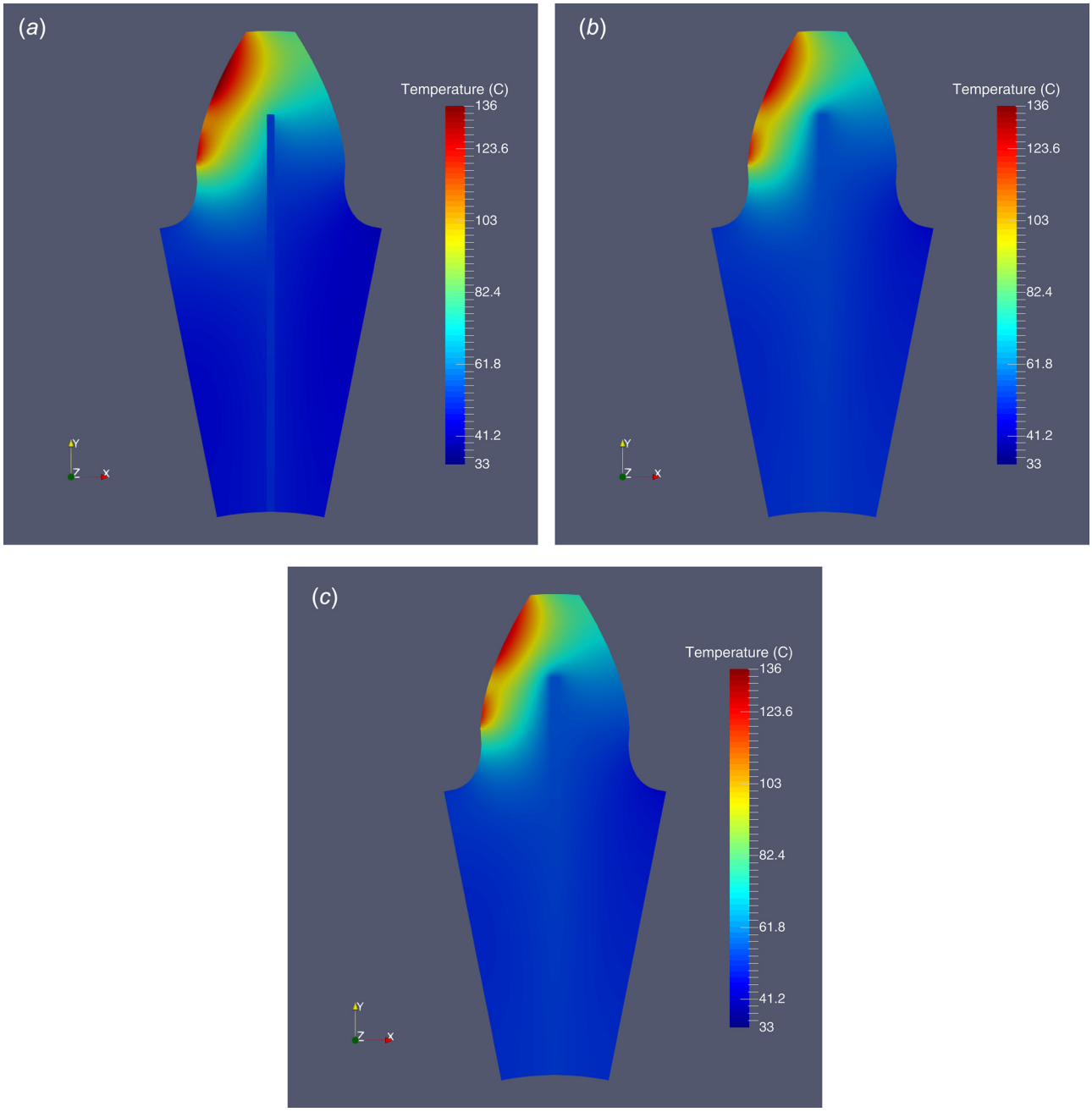

Fig. 6 Maximum and minimum temperature for an aluminum insert: (*a*) 0.1 MPa ($T_{max} = 135.2\,^{\circ}C$, $T_{min} = 33.0\,^{\circ}C$), (*b*) 10 MPa ($T_{max} = 128.7\,^{\circ}C$, $T_{min} = 34.9\,^{\circ}C$), and (*c*) 50 MPa ($T_{max} = 128.3\,^{\circ}C$, $T_{min} = 35.0\,^{\circ}C$)

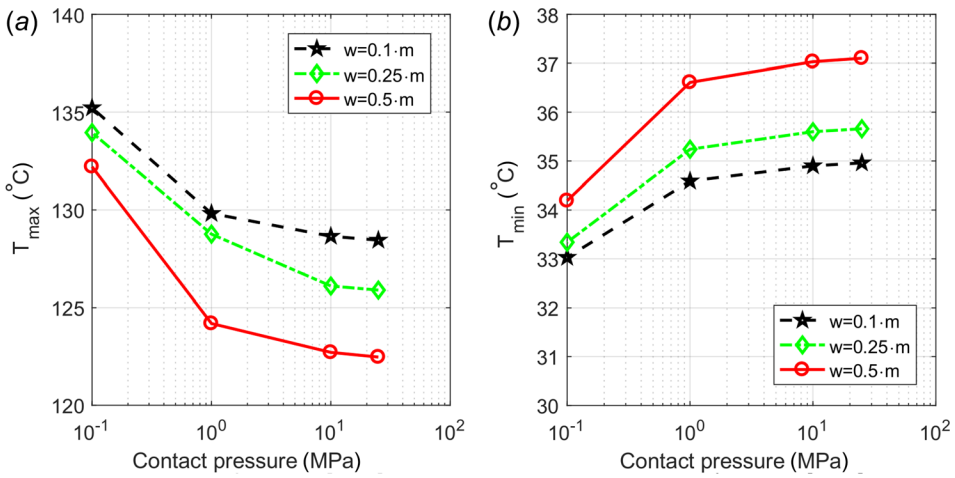

Fig. 7 Maximum and minimum temperature versus plate width *w*: (*a*) maximum temperature for each plate width and (*b*) minimum temperature for each plate width

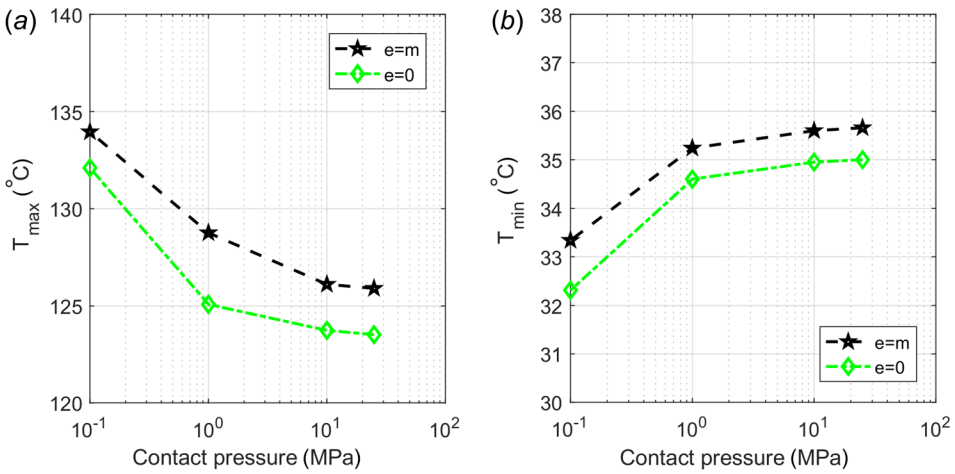

Fig. 8 Maximum and minimum temperature versus lateral gap *e*: (*a*) maximum temperature for each lateral gap and (*b*) minimum temperature for each lateral gap

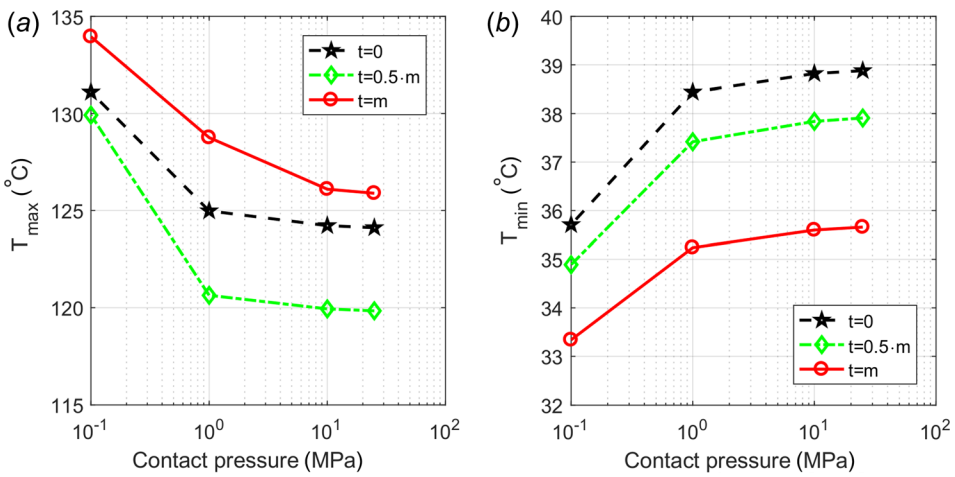

Fig. 9 Maximum and minimum temperature versus tip gap *t*: (*a*) maximum temperature for each tip gap and (*b*) minimum temperature for each tip gap

Based on these simulation results, the following analysis will focus on the influence of the insert geometry instead of the interface pressure, since the heat evacuation capacity is almost equal for 10 MPa to 50 MPa. Furthermore, it is realistic to believe that a contact pressure above 10 MPa is assured by conventional polymer molding technologies.

5.1.3 Influence of the Plate Width (w). Increasing the plate width (see Fig. 1) promotes the reduction of the maximum temperature and increases the minimum temperature as shown in Fig. 7. The increase of the plate width increases also the contact area between POM and aluminum which is important to assure better heat evacuation.

5.1.4 Influence of the Lateral Gap (e). Decreasing the lateral gap (see Fig. 1) will decrease the maximum temperature as presented in Fig. 8(*a*). The contact area increases and the heat evacuation increases as well. However, the minimum temperature will decrease (see Fig. 8(*b*)) because the plate reaches the gear tooth sides and the air convection occurs directly on the plate. Even in a small area, this is enough to decrease both the maximum and the minimum temperature.

5.1.5 Influence of Tip Gap (t). Decreasing the gap t (see Fig. 1) promotes the reduction of the maximum temperature (see Fig. 9(*a*)) if the gap is higher than zero. For the particular case of $t = 0$, the plate works like a thermal barrier and the heat generated in the meshing surface accumulates in one side of the gear. The lower the gap t, the higher the minimum temperature is, as shown in Fig. 9(*b*).

5.2 Best Compromise. The simulation results showed that copper is the most effective material to reduce the maximum temperature of the POM gear tooth. In comparison with the temperature results for a standard POM gear, a maximum decrease of 8.1% is achieved, although the minimum temperature increases. However, as shown in Table 6, the mass increment using a copper insert is higher than using an aluminum insert, while the temperature reached by aluminum insert is quite similar. Among the three materials analyzed (aluminum, copper and steel), the aluminum insert exhibits the best compromise between mass, heat conduction, manufacturing possibilities, and cost.

The insert width (w) as well as the lateral gap (e) and tip gap (t) presented a clear effect on the maximum operating temperature. The shape of the insert should be modified in order to increase the contact area or to position it closer to the tooth contact zone in order to improve thermal evacuation.

6 Other Insert Geometries

For the following calculations, the insert material was assumed to be aluminum according to the conclusions of Sec. 5.2.

A plate like geometry insert with the following properties was designed for the present comparison: $w = m/4 = 1.125$ mm, $e = 0$ mm, and $t = m = 4.5$ mm. A hybrid gear tooth with a plate insert is presented in Fig. 10(*a*).

The addition of a horizontal plate to the initial simple plate insert allows to create a T-profile insert as shown in Fig. 10(*b*). The inclusion of a horizontal plate to allow a closer proximity to the maximum temperature location on the meshing surface. For this comparative study, the geometry has the following characteristics: $w = m/4 = 1.125$ mm, $e = 0$ mm, $t = m = 4.5$ mm. and the width of the horizontal plate is $w_h = m/4 = 1.125$ mm.

Since the maximum operating temperature is achieved in the transition from two to one tooth and from one to two teeth, a double T-profile was created. The profile is inspired by the T-profile but with the purpose to reach the points with the highest operating temperature along the path of contact (root and tip of the gear tooth). The geometry used for this study has the optimized geometry with $w = m/10 = 0.450$ mm, $e = 0$ mm, $t = m/2 = 2.250$ mm, and the width of the horizontal plates is $w_h = m/4 = 1.125$ mm.

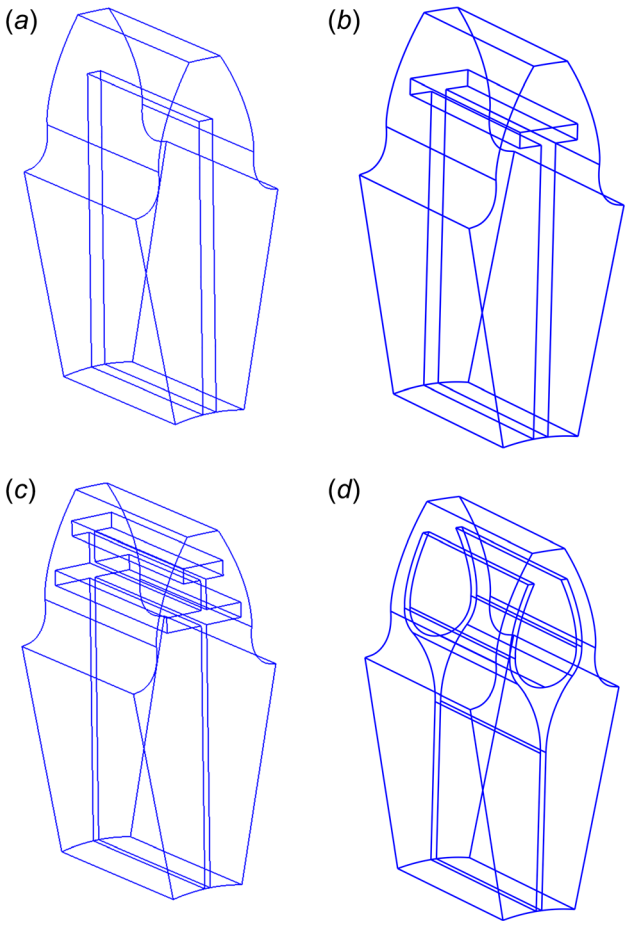

Fig. 10 Different insert geometries with $e = 0$ mm. (*a*) Plate: $w = 1.125$ mm, $t = 4.5$ mm. (*b*) T-profile: $w = 1.125$ mm, $t = 4.5$ mm, and $w_h = 1.125$ mm. (*c*) Double T-profile: $w = 0.450$ mm, $t = 2.250$ mm, and $w_h = 1.125$ mm. (*d*) Involute: $w = 0.450$ mm, $t = 2.250$ mm.

Table 7 Mass for a hybrid pinion tooth (calculated)

Profile	Insert mass (g)	Total mass (g)
POM without insert	—	4.208
Plate	0.924	4.653 (+10.6%)
T-profile	1.067	4.722 (+12.2%)
Double T-profile	0.781	4.584 (+8.9%)
Involute	0.75	4.570 (+8.6%)

The hybrid gear tooth with a double T-profile is shown in Fig. 10(*c*).

Going a little bit further, an involute insert profile that follows the same shape of the meshing tooth would potentially improve the thermal conduction within the gear body. The involute profile presents the following geometric characteristics:

Table 8 Temperature evaluation for each insert geometry (25 MPa)

Geometry	T_{max} (°C)	T_{min} (°C)
POM without insert	139.4	22.3
Plate	123.5 (−11.4%)	35.0 (+57.1%)
T-profile	115.9 (−16.9%)	37.6 (+68.7%)
Double T-profile	100.7 (−27.8%)	40.1 (+82.6%)
Involute	99.6 (−28.3%)	42.3 (+89.7%)

Table 9 Contact area (mm^2) between metallic insert and polymer

Plate	623.79
T-profile	718.29 (+15.1%)
Double T-profile	922.79 (+47.9%)
Involute	971.99 (+55.8%)

$w = m/10 = 0.450$ mm, $e = 0$ mm, and $t = m/2 = 2.250$ mm. Figure 10(*d*) shows the hybrid gear tooth with an involute profile insert.

6.1 Influence of the Insert Geometry on the Tooth Mass. The mass evaluation for the four insert profiles is presented in Table 7.

It is possible to conclude that the total mass of the gear tooth with the different insert profiles does not change that much, the maximum mass corresponds to the T-profile (an increment of 12.2%, increasing from 4.208 g to 4.722 g the total tooth mass when compared with a POM gear without insert). In order to compare the effectiveness of each geometry to evacuate heat, the insert mass is kept similar.

6.2 Influence on Tooth Temperature. Table 8 shows maximum and minimum temperatures for each insert geometry. The comparison to the standard POM gear is given in terms of maximum temperature reduction and minimum temperature increment. It is possible to notice that, using the Involute profile or the double T-profile, the reduction in maximum temperature is about 28% (a reduction from 139 °C to 101 °C is predicted). However, the

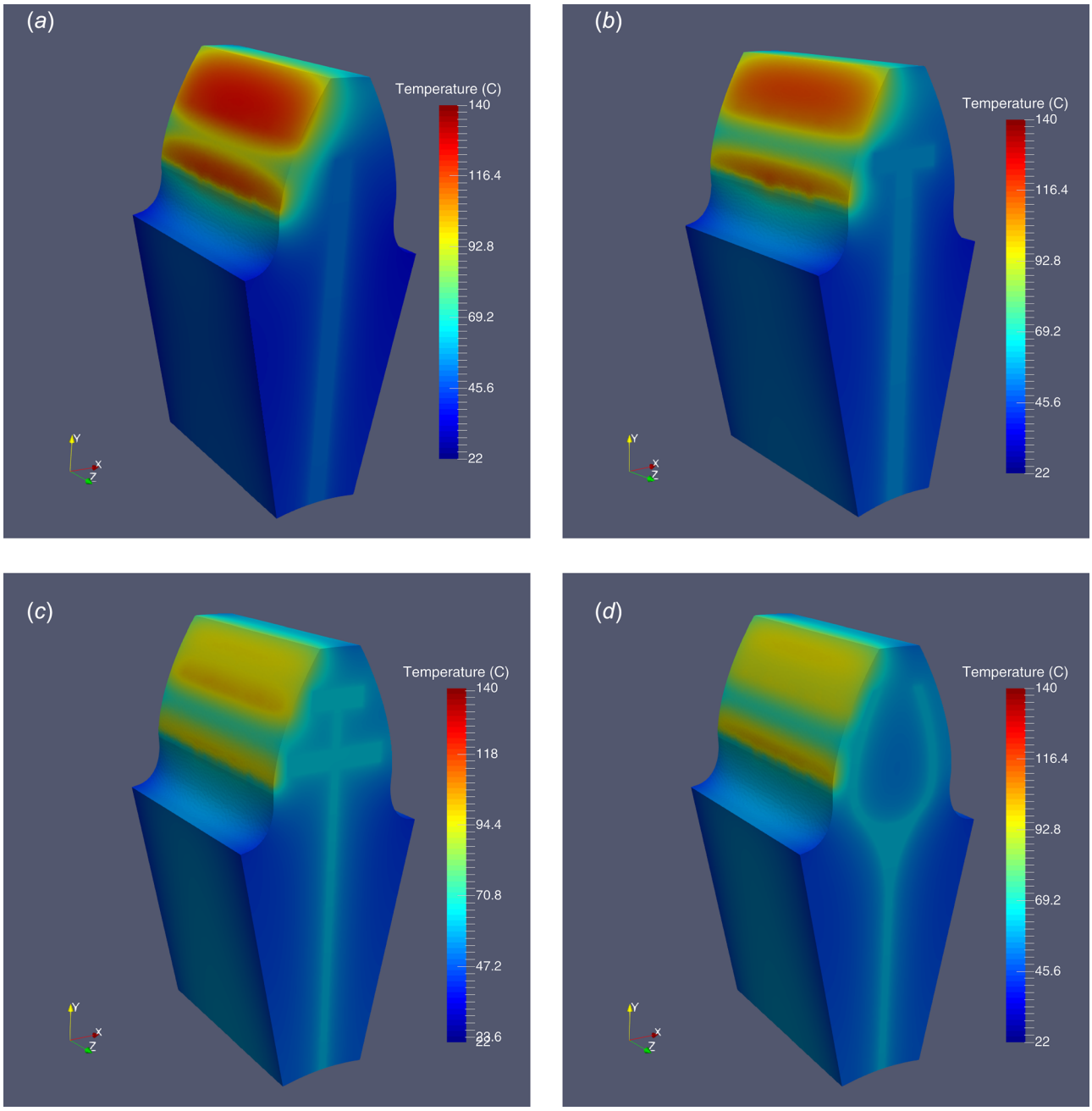

Fig. 11 Temperature distribution for different insert geometries (25 MPa): (*a*) Plate ($T_{max} = 123.5\,^{\circ}C$, $T_{min} = 35.0\,^{\circ}C$), (*b*) T-profile ($T_{max} = 115.9\,^{\circ}C$, $T_{min} = 37.6\,^{\circ}C$), (*c*) Double T-profile ($T_{max} = 100.7\,^{\circ}C$, $T_{min} = 40.7\,^{\circ}C$), and (*d*) Involute ($T_{max} = 99.6\,^{\circ}C$, $T_{min} = 42.3\,^{\circ}C$)

minimum temperature increases 90% and 83% for involute and double-T, respectively. The reduction of maximum temperature when using a plate or T-profile insert is much smaller than the most complex geometries, 11% and 17%, respectively. The T-profile was able to evacuate more heat than a simple plate insert because the heat evacuation from the meshing surface is better if the insert is closer to the surface.

The double T-profile, as expected, improves the heat evacuation in comparison to the T-profile insert because the inserts are close to the maximum heat generation locations along the path of contact.

Finally, the Involute profile insert was the best solution, with the highest reduction of the maximum temperature because it reaches the closest position to the meshing surface promoting an efficient heat evacuation.

It is important to note that, no matter the profile insert used, the maximum temperature decreases but the minimum temperature always increases in comparison to the standard POM gear.

The results suggest that the heat evacuation capacity is closely related to the contact area between the polymer and the insert and the position of the insert within the polymer body. Table 9 shows the contact area for each insert geometry and how the maximum temperature is lower for the insert geometries with higher contact area. The mass increase is shown for each insert type (see Table 7). It can be concluded that there is a link between contact area and maximum operating temperature, but no correlation between mass and maximum operating temperature.

The temperature distribution along the hybrid gear tooth for different insert geometries is shown in Fig. 11 for a contact pressure of 25 MPa. The simulation results show that the insert temperature increases as the heat conduction to the insert occurs, i.e., the maximum temperature decreases because the insert temperature increases which shows that better heat evacuation is taking place (double T-profile and involute). The double T-profile and the involute insert geometries show the most homogeneous temperature distribution within the hybrid gear tooth.

It was possible to conclude with the simulations that the implementation of an aluminum insert will decrease the maximum temperature and possibly enhance the mechanical properties of the polymer.

6.3 Study Limitations. The present work presents some limitations, i.e., only thermal analysis is presented and no structural analysis is available; the manufacturing processes are assumed to be precise enough to assure a reasonable contact pressure between the polymer gear and the metallic insert (>10 MPa).

The study focused only on three different insert material alternatives: aluminum, copper, and steel, allowing to cover a wide range of thermal conductivities (41–401 W m^{-1} K^{-1}). After the simulations, aluminum was found to present a better compromise over copper and steel in terms of mass, thermal behavior, manufacturing processes, and possible costs. However, the thermal conductivity of aluminum is quite dependent on the manufacturing process. The present study intends to be qualitative and if any other material with thermal conductivity similar to the one assumed for aluminum in the present work is used as insert, theoretically, similar results can be achieved.

The geometry is mandatory in order to decrease the maximum operating temperature on the hybrid polymer gear. This work showed that the contacting area as well as the geometry is equally important to improve thermal behavior.

The geometries studied are just possibilities and the exact geometry to be used in practice should be designed according to the manufacturing limitations and structural analysis. However, the structural behavior of the polymer-metal tooth still needs to be analyzed.

The viscoelastic losses were disregarded, but certainly have an impact in the bulk temperature results that were presented.

7 Conclusions

The possibility of using a metallic insert in polymer gears in order to improve their thermal behavior and decrease the bulk temperature of the polymer was studied. The following conclusions were achieved:

- A metallic insert is effective to decrease the bulk temperature of polymer gears.
- Aluminum presents the best compromise between thermal behavior, weight, and manufacturing possibilities.
- The insert geometry has a fundamental importance in the capacity to evacuate heat from the contacting surface.
- The numerical model implemented allows to study the influence of materials and insert geometry on a gear contact problem taking in consideration the thermal aspects.
- The results show that an aluminum insert increases the mass by 9% in comparison with a standard polymer gear but it decreases the maximum operating temperature by 28%.

Acknowledgment

The authors gratefully acknowledge the funding supported by National Funds through Fundação para a Ciência e Tecnologia (FCT), under the project NORTE-01-0145-FEDER-000022 - SciTech - Science and Technology for Competitive and Sustainable Industries, cofinanced by Programa Operacional Regional do Norte (NORTE2020), through Europeu de Desenvolvimento Regional (FEDER) and LAETA under the project UID/EMS/50022/2013.

Nomenclature

a = center distance (mm)
a_i = distributed contact spot radius (m)
A_a = apparent contact area (m^2)
A_r = real contact area (m^2)
b = gear face width (mm)
b_i = distributed flux tube radius (m)
c = heat capacity (J kg^{-1} K^{-1})
C_c = contact dimensionless conductance
d = gear pitch diameter (mm)
d_a = gear addendum diameter (mm)
e = lateral gap (mm)
E = Young's modulus (Pa)
E^* = effective Young's modulus (Pa)
E_{poly} = polymer Young's modulus (Pa)
h_c = contact heat transfer coefficient (W m^{-2} K^{-1})
h_g = gap heat transfer coefficient (W m^{-2} K^{-1})
h_{rad} = radiation heat transfer coefficient (W m^{-2} K^{-1})
h_{tc} = thermal contact heat transfer coefficient (W m^{-2} K^{-1})
H_e = elastic microhardness (Pa)
H_{ep} = elasto-plastic microhardness (Pa)
H_p = plastic microhardness (Pa)
H_{poly} = polymer elastic contact hardness (Pa)
H_{vick} = Vickers microhardness (Pa)
k = thermal conductivity (W m^{-1} K^{-1})
k_s = effective thermal conductivity (W m^{-1} K^{-1})
L = assessment length (mm)
m = gear module (mm)
m_a, m_1, m_2 = absolute asperity slope
m_s = effective absolute asperity slope
n = rotational speed (rpm)
P = contact pressure (Pa)
Q = heat flux (W)
R_a = average surface roughness (μm)
R_{si} = thermal contact resistance of a contact spot (m^2 K W^{-1})
R_{tc} = thermal contact resistance (m^2 K W^{-1})
S_f = yield stress (Pa)
t = tip gap (mm)
T_B = bulk temperature (°C)

x_z = gear profile shift
w = plate width (mm)
w_h = horizontal plate width (mm)
z = gear number of teeth
α = gear pressure angle (deg)
ε = ratio between the real area and apparent area of contact
ϵ_α = transverse contact ratio
μ = coefficient of friction
$\psi_{ci}, \psi_{ci_1}, \psi_{ci_2}$ = mean and contact spot constriction radius (m)
ρ = density (kg m^{-3})
$\sigma, \sigma_1, \sigma_2$ = root-mean-square roughness (μm)
σ_s = effective root-mean-square roughness (μm)
υ = Poisson's ratio

Appendix A: Plastic Contact Model (CMY)

Yovanovich [22,27] was able to predict the thermal contact resistance assuming that the strain of the contacting asperities is large, implying that the plastic deformation of the asperities occurs during the first loading of the contacting surfaces and that the contacting asperities of the softer surface will have plastic deformation.

The ratio between the real area of contact and the apparent area of contact is proportional to the fraction of the apparent contact pressure (P) and the microhardness of the softer surface (H_p).

The dimensionless thermal contact conductance is given by the Eq. (A1):

$$C_c = \frac{h_c \cdot \sigma_s}{k_s \cdot m_s} = 1.25 \cdot \left(\frac{P}{H_p}\right)^{0.95} \tag{A1}$$

Yovanovich introduced the concept of microhardness which is present on a surface layer. The microhardness is dependent on the depth of the indentation according to $H_{\text{vick}} = c_1 \cdot (d_v/d_0)^{c_2}$ and the relation between contact pressure and microhardness is given in Eq. (A2)

$$\frac{P}{H_p} = \left[\frac{P}{c_1 \cdot (1.62 \cdot (\sigma_s/m_s))^{c_2}}\right]^{1/(1+0.071c_2)} \tag{A2}$$

Appendix B: Elasto-Plastic Model (SY)

Sridhar and Yovanovich [37] were able to describe a wide range of materials' behavior from the elastic model studied by Mikic [28] to the plastic model by Cooper and Yovanovich [27]. The relationship between the contact areas and the contact pressure and elasto-plastic microhardness is given by Eq. (B1) [37], where the nondimensional contact strain is $\varepsilon_c = 1.67 \cdot E^* m_s / S_f$

$$H_{\text{ep}} = \frac{2.76 \cdot S_f}{\left[1 + \left(\frac{6.5}{\varepsilon_c}\right)^2\right]^{\frac{1}{2}}} \tag{B1}$$

To calculate the yield/flow stress S_f and the elasto-plastic microhardness (H_{ep}) there is the need to use an iterative procedure until the value converges, starting with an initial guess of H_{ep} as $\sqrt{H_p \cdot H_e}$ (Eqs. (B2)–(B8))

$$S_f = \frac{1}{2.76\sqrt{\frac{1}{H_{\text{ep}}^2} - \frac{1}{H_e^2}}} \tag{B2}$$

$$\varepsilon_c = 1.67 \cdot \frac{E^* m_s}{S_f} \tag{B3}$$

$$f_{\text{ep}} = \frac{\left[1 + \left(\frac{6.5}{\varepsilon_c}\right)^2\right]^{0.5}}{\left[1 + \left(\frac{13.0}{\varepsilon_c}\right)^{1.2}\right]^{\frac{1}{1.2}}} \tag{B4}$$

$$\varrho = \sqrt{2} erfc^{-1} \cdot \left(\frac{1}{f_{\text{ep}} \cdot \varepsilon_c} \cdot \frac{2P}{H_{\text{ep}}}\right) \tag{B5}$$

$$a_m = \sqrt{\frac{8 \cdot f_{\text{ep}} \cdot \varepsilon_c}{\pi}} \frac{\sigma_s}{m_s} \exp\left(\frac{\varrho^2}{2}\right) erfc\left(\frac{\varrho}{\sqrt{2}}\right) \tag{B6}$$

$$d_v = \sqrt{2\pi} \cdot a_m \tag{B7}$$

$$H_{\text{ep}} = \frac{H_{\text{vick}}}{0.9272} \tag{B8}$$

where H_{vick} is the Vickers microhardness given by $H_{\text{vick}} = c_1 \cdot d_v^{c_2}$.

The geometrical parameter n_{cb} is calculated in the same way as in the past two models, however, the dimensionless thermal contact conductance for $\varepsilon_c < 5$ is given by the Eq. (B9):

$$C_c = \frac{h_c \cdot \sigma_s}{k_s \cdot m_s} = 1.54 \cdot \left(\frac{P}{H_{\text{ep}}}\right)^{0.94} \tag{B9}$$

References

[1] Terashima, K., Tsukamoto, N., and Nishida, N., 1986, "Development of Plastic Gear for Power Transmission (Economical Methods for Increasing Load-Carrying Capacity)," Bull. JSME, **19**(247), pp. 256–259.
[2] Terashima, K., Tsukamoto, N., and Nishida, N., 1986, "Development of Plastic Gears for Power Transmission (Design on Load-Carrying Capacity)," Bull. JSME, **29**(250), pp. 1326–1329.
[3] Lourenço, A. F., 2015, "Testing of Low-Loss Polymer Gears," Master thesis, Faculdade de Engenharia da Universidade do Porto, Porto, Portugal.
[4] Hubert, T., Bauser, M., Hasl, C., Tobie, T., and Stahl, K., 2015, "Load Carrying Capacity of Cylindrical Plastic Gears," International Conference on High Performance Plastic Gears, pp. 1183–1190.
[5] Terashima, K., Tsukamoto, N., Nishida, N., and Shi, J., 1986, "Development of Plastic Gear for Power Transmission: Abnormal Wear on the Tooth Root and Tooth Fracture Near Pitch Point," Bull. JSME, **29**(251), pp. 1598–1604.
[6] Cheewawuttipong, W., Fuoka, D., Tanoue, S., Uematsu, H., and Iemoto, Y., 2013, "Thermal and Mechanical Properties of Polypropylene/Boron Nitride Composites," Energy Procedia, **34**, pp. 808–817.
[7] Wirth, M. S., and Seidler, R. T., 2015, "Determination of Load Carrying Capacity Characteristic Values for Plastic Gears," International Conference on High Performance Plastic Gears, pp. 1273–1282.
[8] Höhn, B.-R., Michaelis, K., and Vollmer, T., 1996, "Thermal Rating of Gear Drives: Balance Between Power Loss and Heat Dissipation," American Gear Manufacturers Association, Alexandria, VA, Technical Paper No. AGMA 96FTM8.
[9] Höhn, B., Michaelis, K., and Wimmer, A., 2007, "Low Loss Gears," Gear Technology, Elk Grove Village, IL, pp. 28–35.
[10] Magalhães, L., Martins, R., Oliveira, I., and Seabra, J., 2012, "Comparison of Tooth Profiles and Oil Formulation Focusing Lower Power Losses," Proc. Inst. Mech. Eng., Part J, **226**(6), pp. 529–540.
[11] Fernandes, C., Martins, R., and Seabra, J., 2014, "Torque Loss of Type C40 FZG Gears Lubricated With Wind Turbine Gear Oils," Tribol. Int., **70**, pp. 83–93.
[12] Fernandes, C., Marques, P., Martins, R., and Seabra, J., 2014, "Gearbox Power Loss—Part II: Friction Losses in Gears," Tribol. Int., **88**, pp. 309–316.
[13] Fernandes, C., Marques, P., Martins, R., and Seabra, J., 2015, "Gearbox Power Loss—Part III: Application to a Parallel Axis and a Planetary Gearbox," Tribol. Int., **88**, pp. 317–326.
[14] Fernandes, C. M., Martins, R. C., and Seabra, J. H., 2016, "Coefficient of Friction Equation for Gears Based on a Modified Hersey Parameter," Tribol. Int., **101**, pp. 204–217.
[15] Pont, D., 2007, "Engineering Polymers for High Performance Filters Engineering Polymers for Nonwoven Applications," Wilmington, DE, pp. 1–2.
[16] Li, J., Zhang, L., and Zhao, Q., 2010, "Comparison and Analysis on Different Finite Element Models of Gear Interfacial Contact Temperature," International Conference on Computer Modeling and Simulation (ICCMS), Sanya, Hainan, Jan. 22–24, pp. 132–136.
[17] Long, H., Lord, A. A., Gethin, D. T., and Roylance, B. J., 2003, "Operating Temperatures of Oil-Lubricated Medium-Speed Gears: Numerical Models and Experimental Results," Proc. Inst. Mech. Eng., Part G, **217**(2), pp. 87–106.
[18] Vulkov, L., Yalamov, P., Wasniewski, J., Chmurawa, M., and John, A., 2001, *FEM in Numerical Analysis of Stress and Displacement Distributions in*

Planetary Wheel of Cycloidal Gear (Lecture Notes in Computer Science, Vol. 1988), Springer, Berlin, pp. 170–175.
[19] Maier, E., Ziegltrum, A., Lohner, T., and Stahl, K., 2017, "Characterization of TEHL Contacts of Thermoplastic Gears," Eng. Res., **81**(2–3), pp. 317–324.
[20] Fernandes, C. C. M., Rocha, D. D. M., Martins, R. C. R., Magalhães, L., and Seabra, J. H. J., 2018, "Finite Element Method Model to Predict Bulk and Flash Temperatures on Polymer Gears," Tribol. Int., **120**, pp. 255–268.
[21] David, G.G., ed., 2002, *Spacecraft Thermal Control Handbook* (Fundamental Technologies, Vol. I), The Aerospace Press/American Institute of Aeronautics and Astronautics, Inc., El Segundo, CA/Reston, VA.
[22] Cooper, M. G., Mikic, B. B., and Yovanovich, M. M., 1969, "Thermal Contact Conductance," Int. J. Heat Mass Transfer, **12**(3), pp. 279–300.
[23] DSPE, 2018, "Thermal Contact Conduction," DSPE Your Precision Portal, Eindhoven, The Netherlands, accessed Oct. 4, 2018, http://www.dspe.nl/knowledge-base/thermomechanics/chapter-1—basics/1-2-heat-transfer/thermal-contact-conduction/
[24] Gibbins, J., 2006, "Thermal Contact Resistance of Polymer Interfaces," Master's thesis, University of Waterloo, Waterloo, ON.
[25] Greenwood, J. A., and Williamson, J. B. P., 1966, "Contact of Nominally Flat Surfaces," Proc. R. Soc. London, **295**(1442), pp. 300–319.
[26] Cetinkale, T. N., and Fishenden, M., 1951, "Thermal Conductance of Metal Surfaces in Contact," International Conference of Heat Transfer, pp. 271–275.
[27] Yovanovich, M. M., 1982, "Thermal Contact Correlations. Progress in Aeronautics and Aerodynamics: Spacecraft Radiative Transfer and Temperature Control," Am. Inst. Aeronaut. Astronaut., **20**, pp. 102–150.
[28] Mikic, B., 1974, "Thermal Contact Conductance: Theoretical Considerations," Int. J. Heat Mass Transfer, **17**(2), pp. 205–214.
[29] Fuller, J. J., and Marotta, E. E., 2001, "Thermal Contact Conductance of Metal/Polymer Joints: An Analytical and Experimental Investigation," J. Thermophys. Heat Transfer, **15**(2), pp. 228–238.
[30] Bergam, T. L., Lavine, A. S., Incropera, F. P., and Dewitt, D. P., 2011, *Fundamentals of Heat and Mass Transfer*, 7th ed., Wiley, New York.
[31] Geuzaine, C., and Remacle, J.-F., 2009, "GMSH: A Three-Dimensional Finite Element Mesh Generator With Built-In Pre- and Post-Processing Facilities," Int. J. Numer. Methods Eng., **79**(11), pp. 1309–1331.
[32] ISO, 2000, "FZG Test Procedures—Part 1: FZG Test Method a/8,3/90 for Relative Scuffing Load-Carrying Capacity of Oils," International Organization for Standardization, Geneva, Switzerland, ISO Standard No. 14635-1, I.
[33] ISO, 2004, "FZG Test Procedures—Part 2: FZG Step Load Test A10/16, 6R/120 for Relative Scuffing Load-Carrying Capacity of High EP Oils," International Organization for Standardization, Geneva, Switzerland, ISO Standard No. 14635-2, I.
[34] ISO, 2005, "FZG Test Procedures—Part 3: FZG Test Method A/2,8/50 for Relative Scuffing Load-Carrying Capacity and Wear Characteristics of Semifluid Gear," International Organization for Standardization, Geneva, Switzerland, ISO Standard No. 14635-3, I.
[35] Marks, L., Baumeister, T., and Avallone, E., 1978, *Marks' Standard Handbook for Mechanical Engineers*, McGraw-Hill, New York.
[36] VDI, 2014, "VDI 2736: Part 2, 2014, Thermoplastic Gear Wheels - Cylindrical Gears - Calculation of the Load-Carrying Capacity," VDI Richtlinien, VDI-Verlag GmbH, Dusseldorf, Germany, VDI Standard.
[37] Sridhar, M. R., and Yovanovich, M. M., 1996, "Elastoplastic Contact Conductance Model for Isotropic, Conforming Rough Surfaces and Comparison With Experiments," ASME J. Heat Transfer, **118**(1), pp. 3–9.